

Bright excitonic multiplexing mediated by dark exciton transition in two-dimensional TMDCs at room temperature

*Shaul Katznelson^{1,3,†}, Bar Cohn^{2,3,†}, Shmuel Sufrin^{2,3,†}, Tomer Amit⁵, Subhrajit Mukherjee¹,
Vladimir Kleiner^{2,3}, Pranab Mohapatra⁴, Avinash Patsha⁴, Ariel Ismach⁴, Sivan Refaely-
Abramson⁵, Erez Hasman^{2,3} and Elad Koren^{1,3*}*

AUTHOR ADDRESS

¹Nanoscale Electronic Materials and Devices Laboratory, Faculty of Materials Science and Engineering, Technion – Israel Institute of Technology, Haifa 3200003, Israel.

²Atomic-Scale Photonics Laboratory, Faculty of Mechanical Engineering, Technion – Israel Institute of Technology, Haifa 3200003, Israel.

³Russell Berrie Nanotechnology Institute, and Helen Diller Quantum Center, Technion – Israel Institute of Technology, Haifa 3200003, Israel.

⁴Department of Materials Science and Engineering, Tel Aviv University, Ramat Aviv, Tel Aviv, 6997801, Israel.

⁵Department of Molecular Chemistry and Materials Science, Weizmann Institute of Science, Rehovot 7610001, Israel.

*email: eladk@technion.ac.il

Supplementary Note 1: Addressing the origin of the B_b- exciton photoluminescence

As addressed in the main text, the origin of the B_b- exciton emerges from the spin orbit coupling (SOC), which induce splitting of both the conduction and the valance band. While being an intrinsic property for TMDs, various parameters can affect the B_b- excitonic emission, particularly pump intensity, substrate, and sample quality. To affirm our proposed model, these factors were addressed. We carried out intensity dependent PL measurements for the CVD grown monolayer MoS₂ with an objective of NA 0.75 shown in Figure 1S(a,b), that were taken at two different focal planes, where the B_b- Figure 1Sa and A_b- Figure 1Sb emission, respectively are dominant. These results indicate that the pump intensity had little to no effect on the measured PL modulation. This implies that the emergence of the B_b- exciton did not occur due to the change in the incident power at different focal planes, but rather due to the altering spatial electric field distribution.

One of the unique characteristics of monolayer TMDs is its sensitivity to the dielectric surrounding, that is facilitated mainly by the substrate. To examine this, we have measured the PL spectra for MoS₂ monolayer on only SiO₂ (microscope slide) and sapphire substrate (Figure S2a and Figure S2b). As opposed to the SiO₂ substrate, on sapphire, the PL emission modulation was not observed, rather giving rise to charge excitons (trions) peak, marked as T, at around 670 (nm); which we attributed to the change in electric field intensity at different focal planes. This indicates that the multiplexing is distinctly substrate selective (Figure S2b). We also note that on the SiO₂ substrate a red-shift occurred to the A_b- emission peak as we move up in the focal plane. This can be similarly explained by the transition from the A_b- to the T due to change of the electric field intensity. In the main text (Figure 2a) a similar experiment is presented, but instead of the only SiO₂ substrate the sample was placed on a spacer of 300 nm SiO₂ on-top of a Si substrate. By comparison, the interference generated from the spacer seems to increase the B_b- to A_b- ratio at the 0 μ m focal plane. Notably, while it is not

the source of the modulation phenomena the spacer interference seems to enhance it. This paves a route to control over the B_b - emission channel, by using various thicknesses of SiO_2 on Si substrates as shown in Figure S3a-c. Here the strongest B_b - emission was achieved for a 300 nm spacer of SiO_2 on Si; henceforth, we used in the main text samples on 300 nm SiO_2 on Si substrate.

Supplementary Note 2: Field effective transistor – MoS_2 monolayer

The gate dependent PL of the field effective transistor (FET) device are demonstrated in Figure 4S. Here, a clear modulation between A_b - and the charge exciton T- at different gate voltage was observed. Additionally, no effect on the B_b - transition was present at the same gate voltages, depicted in Figure 4Sb. Consequently, it is deductible that charge particles are not likely to play an important role in the B_b - excitonic transition. The FET device fabrication was done by wet-transferring a monolayer of MoS_2 onto a prepatterned 300nm SiO_2/Si substrate. E-beam lithography (Raith-eLine) was employed to mark the area for the gold contacts, followed by Cr/Au deposition and resist lift off. Finally, the device was mounted onto a chip carrier followed by wire bonding. The FET measurements were carried out using a semiconductor parameter analyzer (Keysight B1500A) and Confocal Raman microscope (WiTec) using an objective of NA=0.45. The gate voltage V_G was applied through the back-side conducting Si and a 300-nm thick SiO_2 layer served as the gate dielectric. The optical image of the connected monolayer MoS_2 is shown in Figure 4Sc.

Supplementary Note 3: Thermal dependent photoluminescence of MoSe₂

PL measurements for monolayer MoSe₂ on 300nm SiO₂/Si substrate were conducted at two temperatures extrema *i.e.* at 298K and at 125K (Figure S5a,b) similar to Figure 3a,b in the main text. A similar trend is observed, showing the B_b- excitonic peak decrease at lower temperature. Furthermore, the B_b- emission is much more profound than what seen for MoS₂ in Figure 3a,b. We note, that for all measurements a certain blue-shift (with decrease in focal z-position) had consistently appeared for the B_b- exciton emission peak, though its origin is still not fully understood.

At Figure S5b a broadening occurs around the A_b- transition. While counter intuitive, as in lower temperature inhomogeneous broadening decreases, the origin of the broadening arise due to the lapping emission spectra from the A_b- and the T transitions, shown for both temperature comparably in Figure S5c,d. As a result, the contribution of T transitions to the spectrum was not considered in the calculation for Figure 3d.

Supplementary Note 4: Raman characterization

We have measured the Raman spectra at different focal plane positions. The characteristic vibrational phonon modes of MoS₂ include the in-plane E_{2g}^1 mode, and the out-of-plane A_{1g} mode (Figure 6Sb). Figure 6Sa shows the normalized Raman spectra at different focal planes (normalized to the A_{1g} peak at 403 cm⁻¹), confirming the monolayer nature of the sample with a separation of ~19 cm⁻¹ between the two Raman modes. Moreover, using an objective with a NA of 0.75 it is evident that the ratio between the A_{1g} and the E_{2g}^1 modes alters with the focal plane, indicating a change in the polarization distribution of the excitation field at different focal planes.

Supplementary Note 5: Chromatic aberration in the confocal microscopy

In confocal microscopy, the longitudinal chromatic aberration induces wavelength dependent focal planes. Hence, the ratio of the B_b/A_b exciton emission is anticipated to change due to chromatic aberration in addition with its modulation due to in- and out-of-plane excitation. In contrast with our proposed dark exciton elevator modulation, the chromatic aberration is temperature independent and will similarly affect the measured B_b/A_b excitonic emission at low temperatures. Thus, the fact that we observed only a minor modulation at low temperature indicates that the chromatic aberration in our setup could be neglected. To demonstrate this, we considered that the observed B_b/A_b exciton emission at low temperature is solely induced by chromatic aberration. Accordingly, the B_b/A_b exciton emission at room temperature was corrected by scaling the measured data according to the low temperature modulation (Figure S7). The corrected modulation profile indicates that the chromatic aberration is indeed minor at room temperature and only acts as an emphasizing means to the elevator mechanism.

Supplementary Note 6: GW-BSE state mixing in MoS_2 , $MoSe_2$, WS_2 and WSe_2 (Figure 4 c-f)

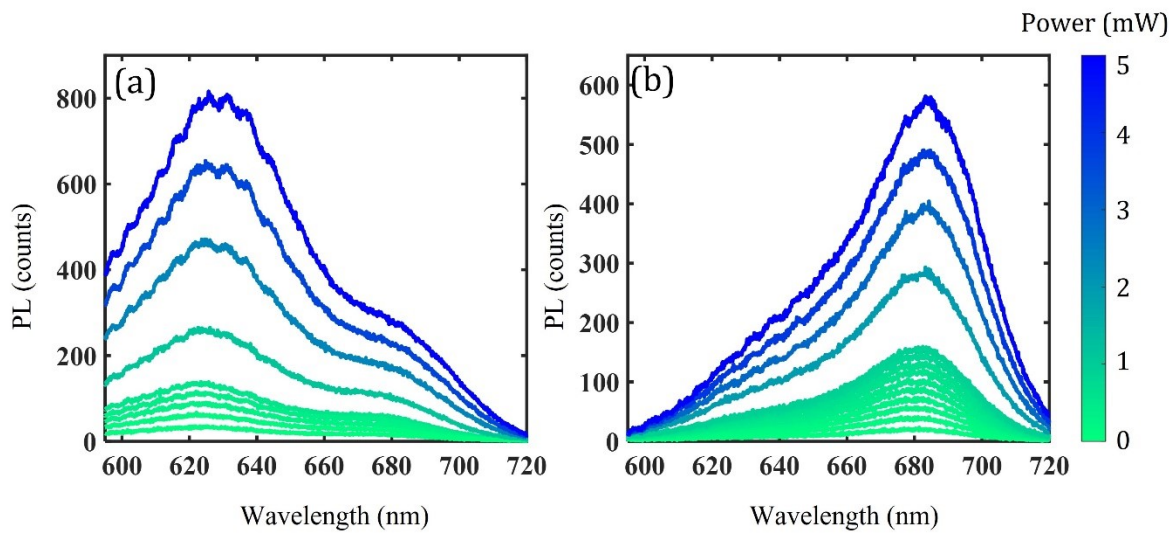
Figure 4c-f in the main text shows exciton transitions divided to separate contributions from electron-hole transitions associated with the A_b , A_d , B_b , B_d . The full GW-BSE data used for the graphically colored lines is given in figure S8.

Supplementary Note 7: Resonant photoluminescence excitation

We have measured the PL spectra of monolayer MoS_2 at two different excitation wavelengths: 532nm and 633nm. Each measurement was conducted for the focal plane at which the B_b -

exciton emission was maximal (note that for 633nm the focal plane was taken relative to the A_b - max signal due to an insignificant modulation of the B_b - spectral region). At 633nm resonant excitation, the lack of B_b - emission feature implies that an upconversion process through the A_d - exciton population is a less plausible explanation for the multiplexing action seen with excitation in 532nm shown in figure S9. It's important to note that the signal in 633nm shown in the spectrum emerges from the exciting laser source fitted with a Lorentzian function.

Supplementary Figure 1:

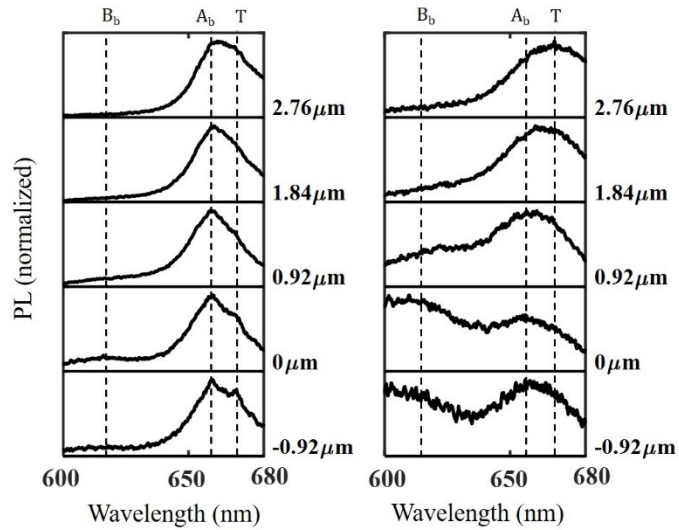


Pump intensity photoluminescence. PL measurements of MoS₂ monolayer on 300nm SiO₂/Si substrate, taken with an objective NA of 0.75 at two focal planes, at which the emission of B_b- (a) and A_b- (b) excitonic emission is dominant. The color scale in the plots indicates the pump intensity depicted by the scalebar on the right. In both graphs, the PL modulation between the B_b- and the A_b- excitonic emission was not observed.

Supplementary Figure 2:

NA 0.75

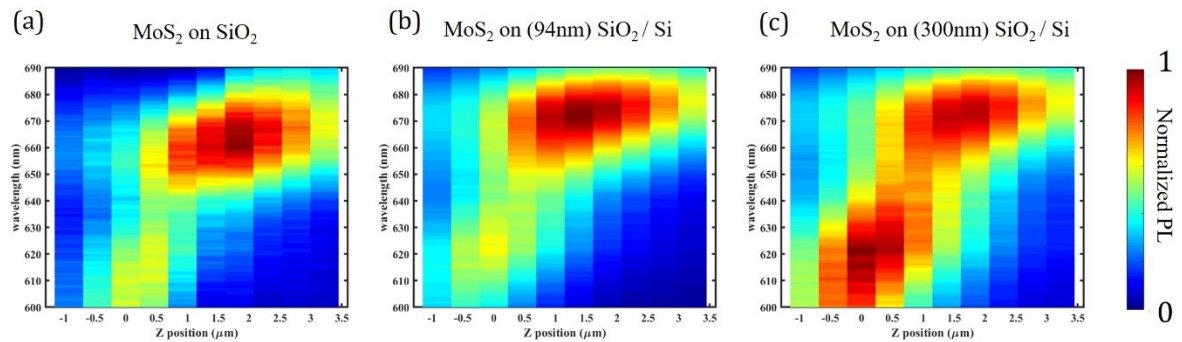
(a) MoS₂ on Sapphire (b) MoS₂ on SiO₂



Substrate dependent photoluminescence from monolayer MoS₂. PL measurements at different focal planes of MoS₂ monolayer. The measurements were taken with an objective NA of 0.75 for two different substrates, **(a)** Sapphire and **(b)** SiO₂ (microscope slide). The PL modulation between the B_b- and the A_b- is clearly shown for the SiO₂ substrate, yet absent on Sapphire.

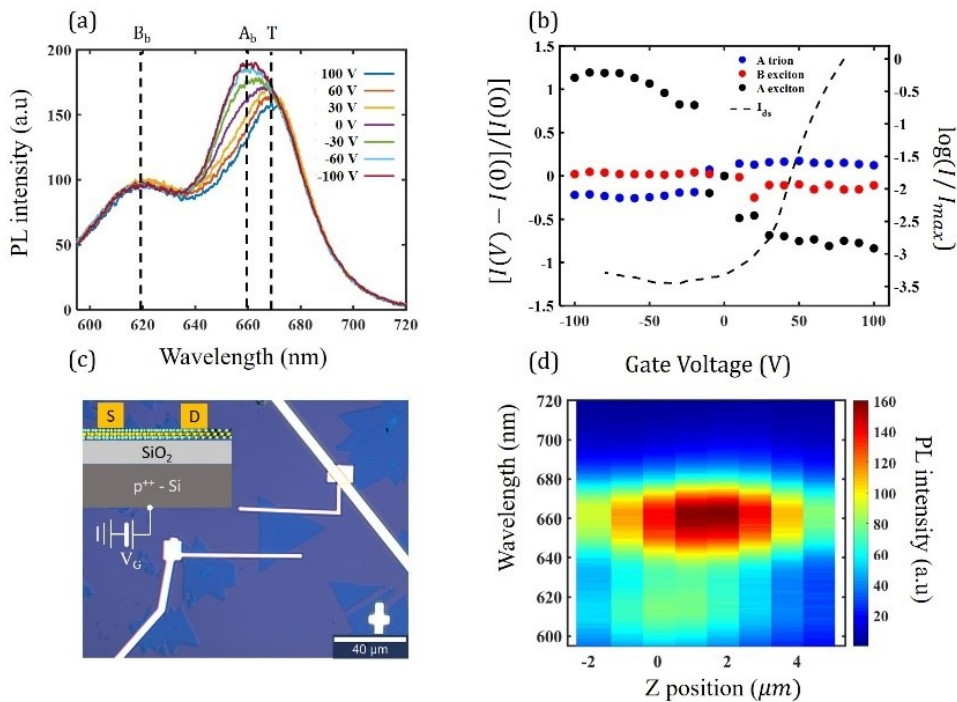
Supplementary Figure 3:

NA 0.75



Spacer enhancement of the B_b- excitonic emission. PL colormap each normalized to the maximum of the set. The measurements were conducted with an objective with NA of 0.75 for three substrates: (a) SiO₂ (glass slide). (b) 94 nm SiO₂ on Si (c) 300 nm SiO₂ on Si. An enhancement is shown for the B_b- excitonic emission for the 300 nm spacer.

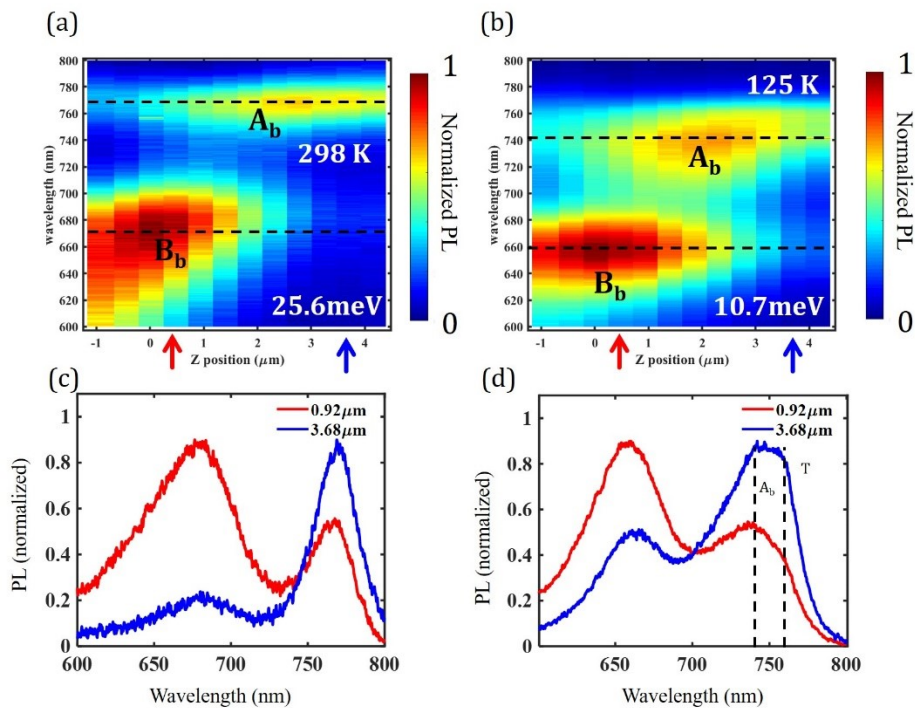
Supplementary Figure 4:



Gate tunable exciton and Trion at room temperature. (a) PL spectra at different gate voltages. Both the natural (marked as A_b- and B_b-) and trion (T) can be observed. (b) Lorentzian fitting for each exciton showing at different voltages a clear evidence for the dominant exciton species. Here the B_b- exciton shows little change. (c) Optical image of the FET device on monolayer MoS₂. The inset depicts the illustration of the device. (d) PL spectrum map of the FET monolayer MoS₂ acquired at different focal plane for NA=0.45.

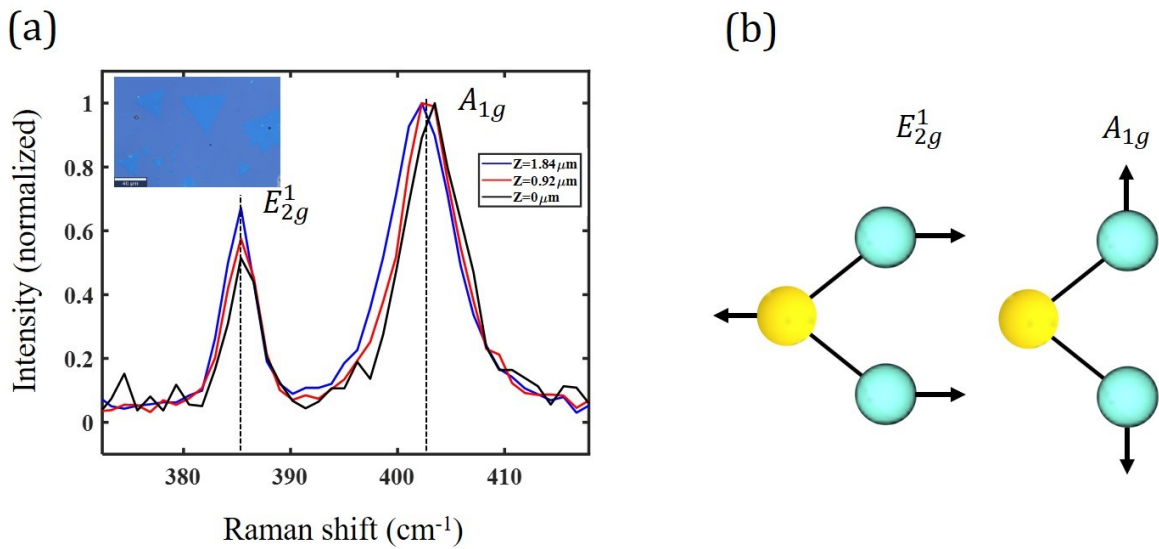
Supplementary Figure 5:

NA 0.45



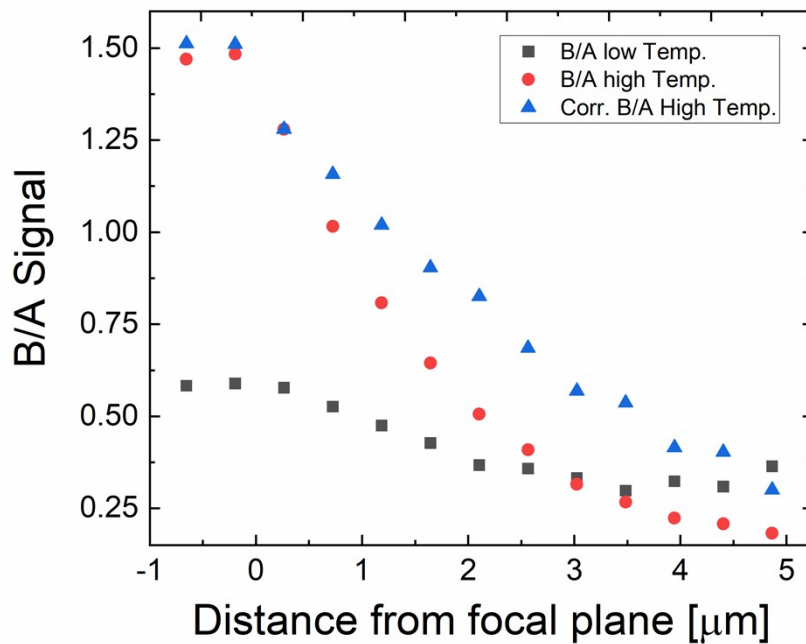
Thermal dependence and PL modulation in monolayer MoSe_2 . PL colormap of monolayer MoSe_2 taken with a NA of 0.45 at different focal planes at 298K (a) and 125K (b). The thermal energy $k_B T$ is noted on the bottom right in each spectrum. PL spectra at two different focal planes for the 298K (c) and 125K (d). The colored arrows at (a,b) marks the corresponding focal planes in (c,d). The graphs exhibit the presence of trions T and their overlapping signal with the A_b -a emission at lower temperature.

Supplementary Figure 6:



Raman modes of monolayer MoS₂. (a) Normalized Raman spectra of a monolayer MoS₂ at different focal plane positions z . The distance between the two Raman modes is $\sim 19 \text{ cm}^{-1}$ corresponding to a single layer of MoS₂. Additionally, a weak modulation can be seen between the two Raman modes. Optical image of the MoS₂ monolayer flakes is shown in the inset. (b) Schematic of the two main vibration modes in a monolayer of TMDC, E_{2g}^1 for in-plane vibrations and A_{1g} for out-of-plane.

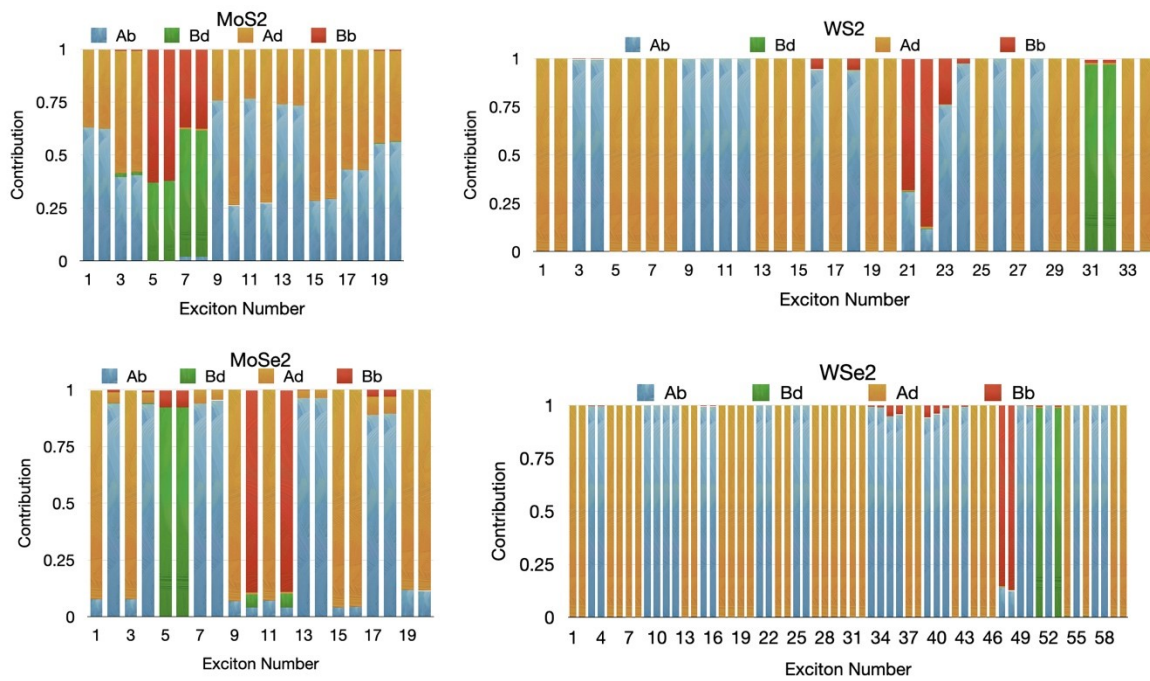
Supplementary Figure 7:



Temperature dependence of B_b/A_b exciton modulation and Chromatic aberration.

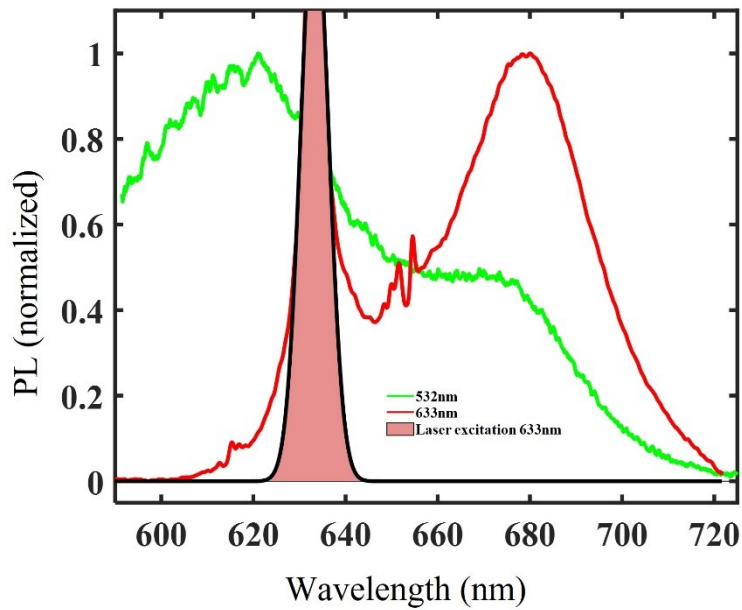
Measured B_b/A_b exciton emission (considering peak areas) as a function of distance from focal plane at both low (black marks) and room temperatures (red marks) of 125K and 298 K, respectively (N.A. = 0.45). The room temperature modulation was further corrected to remove chromatic aberration (blue marks) showing a minor correction in comparison with the original measured data.

Supplementary Figure 8:



GW-BSE exciton transition components for MoS₂, MoSe₂, WS₂, and WSe₂.

Calculated components for the A_b⁻, A_d⁻, B_b⁻, B_d⁻ excitonic transitions for monolayer MoS₂, MoSe₂, WS₂, and WSe₂ systems.



Supplementary Figure 9:

Resonant PL spectroscopy. Normalized PL spectra for MoS₂ for two different excitation frequencies: 532nm (green) and 633nm (red). Each spectrum was accumulated at the B_b- max signal i.e. at the focal plane. For 633nm resonant excitation of the lower energy A excitons, the measured B_b signal was virtually absent. The laser signal is marked by the Lorentzian fit.